Applied Thermal Engineering 250 (2024) 123495

Contents lists available at ScienceDirect

Applied Thermal Engineering

journal homepage: www.elsevier.com/locate/apthermeng

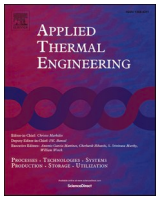

Research Paper

Heat transfer investigation of nano – Encapsulated phase change materials (NEPCMs) in a thermal energy storage device

P. Sudarsana Reddy [a,*], P. Sreedevi [a], Mohammad Ghalambaz [b]

[a] Department of Mathematics, Rajeev Gandhi Memorial College of Engineering and Technology, Nandyal - 518501, A.P, India
[b] College of Engineering, Almaaqal University, Basra 61003, Iraq

ARTICLE INFO

Keywords:
NEPCMs
Heat capacity ratio
Stefan number
Radiation
Finite element method
Volume fraction of NEPCMs

ABSTRACT

Phase change natural convection heat transport and flow features of a variety and new types of hybrid nanoliquids, suspension of Nano – encapsulated phase change materials (NEPCMs), within a square cavity is inspected theoretically in this analysis. The capsules are arranged with a shell and a PCM as a core. The shell of this NEPCM prevents the phase change material from the direct interaction of hot fluid and from the leakage. The heat capacity of the suspension contains latent heat generated at the time of phase change. The modeled equations are numerically scrutinized with Finite element method. Variable thermal conductivity parameter ($1 \leq Nc \leq 5$), variable viscosity parameter ($1 \leq Nv \leq 5$), radiation number ($0.5 \geq R \geq 0.1$), Rayleigh parameter ($10^2 \leq Ra \leq 10^3$), volume fraction of NEPCMs ($1\% \leq \phi \leq 5\%$) and fusion temperature ($0.2 \leq \theta_f \leq 1.0$) impact on the patterns of heat capacity ratio, isotherms and velocity lines are examined in detail. The results indicates that, as the volume fraction values of NEPCMs amplifies from 1% to 5% the rates of heat transfer of the nanoliquid magnifies 42% compared to the host fluid. Non – dimensional rates of heat transport magnifies with growing (Ste) values.

1. Introduction

Convection heat transport of nanoliquids inside a square chamber is basically very important in thermal engineering, thermal insulation, energy storage, drying technologies, heat exchangers and many industrial processes. The enrichment of heat transport in host fluids is achieved by suspending nanoparticles of higher thermal conductivity. Several authors [1–10] studied the convective heat transport of different nanoliquids inside a square chamber by taking numerous numbers of influenced parameters.

Phase Change Materials (PCM) are widely employed in handling thermal devices as they have the capability of discharging and storing the energy during their phase conversion. To cool down the overheated electronic appliances and to control the thermal processes of the devices PCMs are frequently utilized. Suspension of NEPCMs in a regular working liquid is promising for preserving of sensitive equipment's like, chipsets in a computer, detectors, laser optical arrangement structures etc. Keeping numerous numbers of applications of NEPCMs, Selimefendigil et al. [11] professed 118% enhancement in the heat transport rates of NEPCM s flow inside a cavity without magnetic field, while with magnetic field it was 95% when the volume fraction of suspended nanoparticle is 0.04. Ghalambaz et al. [12] pondered noticeable heat transport augmentation when the volume fraction of added NEPCMs is greater than 0.03 in their work on heat transport features of suspension of PCMs inside a permeable chamber. Kumar et al. [13] premeditated the enactment of H_2O in glass expatriate pipe solar H_2O radiator in two cases such as with paraffin as PCM and without PCM and ascertained that the dissemination of CeO2 nanoparticles remarkably magnifies the thermal storage features of the paraffin. Sathish kumar et al. [14] scrutinized 14.13% and 12.8% magnification in the latent heat values for discharging and charging process when the value of volume fraction of nanoparticle is 0.75% in their work on thermal energy storage behavior of NEPCMs. Afshar et al. [15] premeditated the significance of entropy generation and heat sink/source on heat transport features of NEPCM s based nanoparticles within a square storage unit and ascertained that the contours of isentropic magnifies with the escalating values of undulation number. Nayak et al. [16] pondered the implication of Christov – Cattaneo heat flux and magnetic field on the flow properties of nanoliquid inside a cold rounded cylinder by considering hot wavy baffle at the middle of the chamber and established that the motion of the NEPCMs nanoliquid denigrates with increasing values of

* Corresponding author.
E-mail address: suda1983@gmail.com (P. Sudarsana Reddy).

https://doi.org/10.1016/j.applthermaleng.2024.123495
Received 24 January 2024; Received in revised form 3 May 2024; Accepted 24 May 2024
Available online 27 May 2024

Nomenclature

g	Gravitational acceleration
Ra	Local Rayleigh number
H	Cavity height
T_h	Hot wall temperature
Cr	Heat capacity Ratio
σ^*	Stephan-Boltzmann constant
$\overline{p}$	Dimensionless pressure
Nc	Conductivity parameter
(x,y)	Coordinate system
f	Non-dimensional fusion temperature
Ste	Stefan number
c_p	Specific heat in constant pressure $\left(\frac{J}{kg}K\right)$
k_f	Base liquid thermal conductivity
T_c	Cold wall temperature
T	Fluid temperature
R	Radiation parameter
Pr	Prandtl number
K^*	Mean absorption coefficient
(u,v)	Velocity components in $x-$ and $y-$ axis
Nu	Nusselt Number
Nv	Viscosity parameter
T_{MR}	Phase change temperature range

Greek symbols

ρ_p	Nanoparticle mass density
ν	Kinematic viscosity
θ	Dimensionless temperature
ρ_f	Fluid density
$(\rho c_p)_p$	Heat capacitance of the fluid
k	Thermal conductivity
δ	Non-dimensional parameter of fusion Range
μ	Fluid viscosity
α_m	Thermal diffusivity of base fluid
φ	Nanoparticle volume fraction
β	Thermal expansion coefficient of the fluid
$(\rho c_p)_{nf}$	Heat capacitance of the nanofluid
Ψ	Dimensionless stream function
λ	Ratio of heat capacity

magnetic parameter. Peng et al. [17] presented a review article on the recent developments of NEPCMs, like, chemical, physical, thermal properties and also analyzed the preparation procedure of shell and core of NEPCMs. Seyyedi et al. [18] studied the heat capacity ratio and isotherms contours behavior of nanoliquid inside a cavity of elliptic shape filled with NEPCMs. Lan et al. [19] premeditated thermal conductivity augmentation of NEPCMs prepared by taking BN/SiO2 as shell and n −Octadecane as core. Alhashash et al. [20] deliberated NEPCMs heat transport features prepared by considering nonadecane as core and polyurethane as shell inside a wavy cavity and sensed that as the value of fusion temperature magnifies the heat transport rates of nano-liquid amplifies within the cavity. Aly et al. [21] pondered that as the values of either fusion temperature or Stefan number magnifies the area occupied by the red ribbon zone denigrates. Dogonchi et al. [22] identified diminution in the contours of streamlines with increasing values of magnetic number in their study on heat transport features of nanoliquid within a chamber packed with porous balls and nano – encapsulated phase change materials. Li et al. [23] detected that Foam/NEPCMs mixture delivers 47% higher wall temperature reduction compared with normal NEPCMs in their study work on heat transport features of NEPCMs. Alizadeh et al. [24] professed 40.9% magnification in the thermal efficiency of the NEPCMs when the volume fraction of suspended SWCNTs is 0.04 in their analysis. Zidan et al. [25] deliberated the contours of heat capacity ratio, isotherms, isoentropic lines behavior within a T- shaped permeable storage unit filled with NEPCMs and double corrugated hot baffles and identified that solidification – melting zone area contrasts with increasing values of fusion temperature. Aly et al. [26] scrutinized that the NEPCMs flow rate inside the closed storing unit deteriorates with escalating value of Darcy number. Doshi et al. [27] pondered the reduction of overall pressure drop and augmentation of heat transfer of water − NEPCMs mixture inside a wavy hybrid microchannel with entropy generation and established diminution in the liquid domain temperature as the values of suspended NEPCMs upsurges. Mandal et al. [28] studied the synthesis and solicitations of paraffin phase change material encapsulated with silica and sensed that efficiency and heat capacity ratio are both augments as the ratio of shell − core amplifies. Hussain et al. [29] presented the import of thermal radiation and wavy wall on flow features of NEPCMs with in a wavy permeable cavity and sensed 153.8% augmentation in the values of average heat transport rates with Rayleigh number. D'Oliveira et al. [30] presented a review on the preparation techniques to make NEPCMs, stability of the NEPCMs, heat transport augmentation techniques by utilizing NEPCMs, etc. Ghalambaz et al. [31,32] examined unsteady and steady natural convection of nano – encapsulated phase change materials disseminated in water heat transport features within a permeable energy storage device filled with glass balls, copper foam and aluminum foam. Khodadadi et al. [33] professed magnification in the charging rate of photo voltaic unit when the volume fraction of NEPCMs augments from 0.01 to 0.04 in the experimental study on the significance of volume fraction of various types of NEPCMs and nanoparticles on efficaciousness of photo voltaic unit. Sadeghi et al. [34] premeditated entropy generation and volume fraction impact on the heat transport and flow analysis of NEPCMs within L – shaped inclined closed unit and sensed 36 % magnification in the average heat transport rates as volume fraction values escalates. Radhakrishnan et al. [35] professed the influence of hybrid nanoliquid made up of silver (Ag) and Graphene nanoplatelet (GNP) on heat transport magnification embedded in a liquid – solid phase change material and found 57 % amplification in thermal conductivity when 1 % of volume fraction of GNP/Ag is suspended in PCM. Very newly, many investigators [36 –40] perceived heat transport and flow features of NEPCMs prepared with different types of cores and shells within thermal energy storage devices.

In all aforementioned studies the combination of magnetic field and thermal radiation impact on flow and heat transport features of NEPCMs is not examined. Hence, we made an attempt to scrutinize heat transport and flow features of thermally radiative nano – encapsulated phase change materials, prepared with non – adecane as core and polyurethane as shell, within a thermal energy storage device by enchanting magnetic field in this analysis. Variable thermal conductivity and variable viscosity are also taken in this analysis. The considered NEPCMs are also treated as additives or change methods to prevent agglomeration. To the author's knowledge the research presented in this investigation is unique.

2. Problem physics and modeling

Fig. 1 depicts physical picture and schematic diagram of the present analysis. As seen, consider a chamber of square type with size H equipped with addition of NEPCMs and water as regular liquid. T_h is the temperature of the left hot perpendicular wall, whereas the temperature

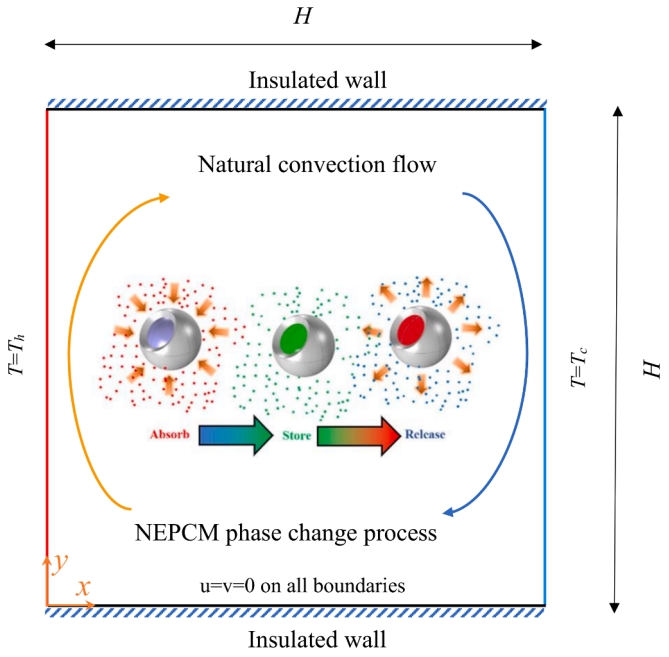

Fig. 1. Flow model and Coordinate system.

of the cold perpendicular right wall is T_c. However, both top and bottom walls are thermally insulated. The nano – encapsulated PCM is prepared with polyurethane as shell and a phase transform material nonadecane as a core. The central part of NEPCMs particles undergoes change of its phase from solid state to liquid state and absorbs/releases its heat in the form of dormant heat energy at the fusion temperature T_f, where $T_c < T_f < T_h$. The combination of regular liquid and NEPCMs are supposed to be in local thermal equilibrium, stable, steady, uniform and incompressible. Also, temperature differences are very less inside the chamber and density of nanoparticles is a function of temperature, the thermophysical properties are independent of temperature and are modeled by Boussinesq approximations. Regular liquids and NEPCMs thermophysical possessions are listed in Table 1. 211 kJ/kg is the latent heat and 32^0C is the fusion temperature of the core of the phase change material. Under the above assumptions, the momentum equations of the mixture in both x and y directions, continuity and energy equations are modeled as follows:

$$\frac{\partial u}{\partial x}+\frac{\partial v}{\partial y}=0 \tag{1}$$

$$u\frac{\partial u}{\partial x}+v\frac{\partial u}{\partial y}=-\frac{1}{\rho_b}\frac{\partial p}{\partial x}+\frac{\mu_b}{\rho_b}\left(\frac{\partial^2 u}{\partial x^2}+\frac{\partial^2 u}{\partial y^2}\right) \tag{2}$$

$$u\frac{\partial v}{\partial x}+v\frac{\partial v}{\partial y}=-\frac{1}{\rho_b}\frac{\partial p}{\partial y}+\frac{\mu_b}{\rho_b}\left(\frac{\partial^2 v}{\partial x^2}+\frac{\partial^2 v}{\partial y^2}\right)+g(\rho\beta)_b(T-T_\infty) \tag{3}$$

$$u\frac{\partial T}{\partial x}+v\frac{\partial T}{\partial y}=\frac{k_b}{(\rho C_p)_b}\left[\frac{\partial^2 T}{\partial x^2}+\frac{\partial^2 T}{\partial y^2}\right]-\frac{1}{(\rho C_p)_b}\left(\frac{\partial q_{rx}}{\partial x}+\frac{\partial q_{ry}}{\partial y}\right) \tag{4}$$

with the following conditions

$v=0, u=0, T=T_h$ at $x=0$.

$v=0, u=0, T=T_c$ at $x=H$.

$v=0, u=0, \frac{\partial T}{\partial y}=0$ at $y=0$.

$$v=0, u=0, \frac{\partial T}{\partial y}=0 \text{ at } y=H. \tag{5}$$

Table 1
Thermophysical possessions of nanoliquids.

	Material	$\rho\left(\frac{Kg}{m^3}\right)$	$C_p\left(\frac{J}{kgK}\right)$	$k\left(\frac{W}{mK}\right)$	$\beta \times 10^{-5}$
Base fluid	Water	997.1	4179	0.613	21
Shell	Polyurethane	721	2037	–	–
Core	Nonadecane	786	1317.7	–	17.28

Based on the density of the common liquid and NEPCM elements, the density of the mixture is demarcated as follows

$$\rho_b=(1-\phi)\rho_f+\phi\,\rho_p \tag{6}$$

Where, the subscript f represents regular liquid and p is related to the NEPCM nanoparticles.

NEPCM nanoparticles density (ρ_p) is the combination of shell density and core density, so its effective density is demarcated as

$$\rho_p=\frac{\rho_s\rho_c(1+\tau)}{\tau\rho_c+\rho_s} \tag{7}$$

Where, τ is the weight ratio of shell – core and is approximately 44.7%, the subscripts c and s represent core and shell. Further, the density of the core of PCM is estimated as the mean of liquid core density and solid core density of PCM. Because the solid core PCM density and liquid core PCM density are different.

Based on the thermal equilibrium between the host liquid and NEPCMs, the specific heat capacity of the suspension is premeditated from the subsequent relation.

$$(C_p)_b=\frac{(C_p)_p\rho_p\phi+(C_p)_f(1-\phi)\rho_f}{\rho_b} \tag{8}$$

The encapsulated nanoparticles contain core and shell complete specific heat capacity in the nonappearance of phase change can be calculated as

$$(C_p)_p=\frac{\left((C_p)_s\tau+\rho_s\rho_c(C_p)_{c,l}\right)}{(\tau\rho_c+\rho_s)\,\rho_p} \tag{9}$$

It is worthy enough to mention that core specific heat capacity in liquid phase is different from the specific heat capacity of core in solid phase. Thus, core PCM specific heat capacity is estimated as the mean of solid and fluid specific heat capacity of the phase change materials and is represented as the subscripts c, l.

As the core of PCM experiences a change of phase, so, the hidden heat energy change of phase should be comprised in the specific heat capacity of NEPCM. For this purpose sinusoidal or triangular and rectangular sketches are available. The sinusoidal profiles will significantly intensifies the convergence criteria by smoothening the variations of $(C_p)_{c,l}$. By considering latent heat and sensible heat of the change of phase material, the total $(C_p)_p$ of the core phase change materials take the subsequent form:

$$(C_p)_p=(C_p)_{l,\,c}+\left\{\frac{\pi}{2}\cdot\left(\frac{h_{sf}}{T_{Mr}}-(C_p)_{l,\,c}\right)\mathrm{Sin}\left(\pi\frac{T-T_f+\frac{T_{Mr}}{2}}{T_{Mr}}\right)\right\}\begin{cases}0, T<T_f-\dfrac{T_{Mr}}{2}\\ 1, T_f-\dfrac{T_{Mr}}{2}<T<T_f+\dfrac{T_{Mr}}{2}\\ 0, T>T_f+\dfrac{T_{Mr}}{2}\end{cases} \tag{10}$$

Where, fixed fusion temperature is T_f and change of phase happens in a very minor temperature period and is considered as T_{Mr}. As T_f results discontinuity in the heat equation, so, rather than considering constant fusion temperature T_f, the middle of T_{Mr} is considered to avoid discontinuity. Furthermore, the core of PCM is itself in solid state if the

temperature of the core is less than the liquefying interval, the core is in fluid state if the temperature of the core is higher than liquefying interval and the core is partly liquefied if the temperature of the core is within the liquefying interval. Since, the value of $\left(\frac{h_{sf}}{T_{Mr}}\right)$ is very large related to $(C_p)_{c,l}$, so, the term $\frac{\pi}{2}.(C_p)_{c,l}$ is easily neglected.

The combination of NEPCM nanoparticle and base liquids thermal volumetric expansion can be modeled as

$$\beta_b = \beta_p\phi + \beta_f(1-\phi) \tag{11}$$

Several theoretic and experiment research works on thermal conductivity and dynamic viscidness of nanoparticles reveals that there is a linear connection among nanoparticles volume fraction and thermal conductivity of the suspended nanoparticles. Also, a similar kind of relation exists between the volume fraction of nanoparticles and dynamic viscidness of the added nanoparticles. Hence, the dynamic viscidness and thermal conductivity of the suspended NEPCMs as a function of volume fraction of nanoparticles are related as follows.

$$\frac{k_b}{k_f} = 1 + Nc\,\phi \tag{12}$$

$$\frac{\mu_b}{\mu_f} = 1 + Nv\,\phi \tag{13}$$

Here, Nv and Nc are the parameters of variable viscidness and variable thermal conductivity. The above relationships are valid only for the nanoliquids whose volume fraction ϕ value is less than 0.5%. Furthermore, as the Nv and Nc values intensify then the values of thermal conductivity and dynamic viscidness of the suspended nano-particles will augment remarkably. In addition, both parameters Nv and Nc are highly influenced by the many parameters of the nanoparticles, like, shape of the nanoparticle, kind of nanoparticles, size of the nanoparticle, kind of the regular liquid, temperature of the regular liquid, volume fraction and ultrasonication time of nanoparticles and others.

Introducing the subsequent non-dimensional variables to transmute the prevailing equations

$$V = \frac{v\,H}{\alpha_f}, Y = \frac{y}{H}, X = \frac{x}{H}, U = \frac{u\,H}{\alpha_f}, \theta = \frac{T - T_c}{T_h - T_c}, P = \frac{p\,H^2}{\rho_f\alpha_f^2} \tag{14}$$

The radiative temperature fluxes q_{ry} and q_{rx} (utilizing Rosseland estimation) is demarcated as

$$q_{ry} = -\frac{4\sigma^*}{3K^*}\frac{\partial T^4}{\partial y}, q_{rx} = -\frac{4\sigma^*}{3K^*}\frac{\partial T^4}{\partial x} \tag{15}$$

The Taylor's series representation of T^4 after omitting higher derivatives about the point T_∞, as T^4 is linearly depending on temperature, is as follows.

$$T^4 \cong 4{T_c}^3T - 3{T_c}^4 \tag{16}$$

After replacing eqn. (16) in eqn. (15), we obtain

$$q_{rx} = -\frac{16{T_c}^3\sigma^*}{3\beta_r}\frac{\partial T}{\partial x}\, q_{ry} = -\frac{16{T_c}^3\sigma^*}{3\beta_r}\frac{\partial T}{\partial y}. \tag{17}$$

The Eqns. (1) – (4) together with boundary conditions Eqn. (5) can take the non – dimensional form

$$U\frac{\partial U}{\partial X} + V\frac{\partial U}{\partial Y} = -\frac{1}{A_1}\frac{\partial P}{\partial X} + \frac{Pr}{A_1}(1 + Nv\,\phi)\left(\frac{\partial^2 U}{\partial X^2} + \frac{\partial^2 U}{\partial Y^2}\right) \tag{18}$$

$$U\frac{\partial V}{\partial X} + V\frac{\partial V}{\partial Y} = -\frac{1}{A_1}\frac{\partial P}{\partial X} + \frac{Pr}{A_1}(1 + Nv\,\phi)\left(\frac{\partial^2 V}{\partial X^2} + \frac{\partial^2 V}{\partial Y^2}\right) + \frac{Ra.\ Pr.\ A2}{A_1}\theta \tag{19}$$

$$Cr.\left(U\frac{\partial\theta}{\partial X} + V\frac{\partial\theta}{\partial Y}\right) = (1 + Nc\,\phi)\left(\frac{\partial^2\theta}{\partial X^2} + \frac{\partial^2\theta}{\partial Y^2}\right) + R\left(\frac{\partial^2\theta}{\partial X^2} + \frac{\partial^2\theta}{\partial Y^2}\right) \tag{20}$$

With related boundary conditions

$$\begin{aligned} &V = 0, \quad U = 0, \quad \theta = 0, \quad \text{when } X = 0.\\ &V = 0, \quad U = 0, \quad \theta = 1, \quad \text{when } X = 1.\\ &V = 0, \quad U = 0, \quad \tfrac{\partial\theta}{\partial Y} = 0 \ \text{when } Y = 0.\end{aligned}$$

$$V = 0, \quad U = 0, \quad \frac{\partial\theta}{\partial Y} = 0 \ \text{when } Y = 1. \tag{21}$$

The dimensionless parameters are demarcated as

$$Ra = \frac{(T_h - T_c)(\rho\beta)_f\, g\, H^3}{\mu_f\alpha_f}, Pr = \frac{(\mu)_f}{\alpha_f\rho_f}, R = \frac{16}{3}\frac{\sigma_e}{B_R}\frac{T_c^3}{K_f},$$

$$A_2 = \phi\left(\frac{\beta_p}{\beta_f}\right) + (1-\phi), A_1 = \phi\left(\frac{\rho_p}{\rho_f}\right) + (1-\phi). \tag{22}$$

Using Eqns. (8) – (10), the heat capacity ratio term (Cr) can be written in non – dimensional form as

$$Cr = \frac{(\rho C_p)_b}{(\rho C_p)_f} = \phi\,\lambda + (1-\phi) + \frac{\phi}{\delta\,Ste}f \tag{23}$$

Where, (λ) is the sensible heat capacity ratio, (Ste) is the Stefan number and (δ) is the non − dimensional phase change bond, which are demarcated as

$$\lambda = \frac{\left((C_p)_{c,l} + \tau\,(C_p)_s\right)\rho_s\rho_c}{\rho_f(C_p)_f(\rho_s + \tau\rho_c)}, Ste = \frac{\rho_f(C_p)_f(T_w - T_c)(\rho_s + \tau\rho_c)}{\rho_c\rho_s h_{sf}}, \delta = \frac{T_{mr}}{(T_w - T_c)} \tag{24}$$

Also, the dimensionless fusion function f is demarcated as

$$f = \left\{\frac{\pi}{2}.\sin\left(\frac{\pi}{\delta}\left(\theta - \left(\theta_f - \frac{\delta}{2}\right)\right)\right)\right\}\begin{cases} 0, \theta < \theta_f - \frac{\delta}{2} \\ 1, \theta_f - \frac{\delta}{2} < \theta < \theta_f + \frac{\delta}{2} \\ 0, \theta > \theta_f + \frac{\delta}{2} \end{cases} \tag{25}$$

Where, θ_f in dimensionless fusion temperature and is defined as

$$\theta_f = \frac{(T_f - T_c)}{(T_w - T_c)} \tag{26}$$

The local Nusselt number at hot wall is demarcated as

$$Nu_y = -\frac{k_b}{k_f}\left(\frac{\partial\theta}{\partial X}\right)_{X=0} \tag{27}$$

The local Nusselt number at cold wall is demarcated as

$$Nu_y = -\frac{k_b}{k_f}\left(\frac{\partial\theta}{\partial X}\right)_{X=1} \tag{28}$$

After applying thermal conductivity ratio Eqns. (27) and (28) takes the form

$$\begin{aligned} Nu_y &= -(1 + Nc\,\phi)\left(\frac{\partial\theta}{\partial X}\right)_{X=0} (\text{Hot wall}), \quad Nu_y \\ &= -(1 + Nc\,\phi)\left(\frac{\partial\theta}{\partial X}\right)_{X=1} (\text{Cold wall}) \end{aligned} \tag{29}$$

The average Nusselt number (Nu) at the hot wall is defined as

$$Nu = (-1 - Nc\,\phi)\int_0^1 \left(\frac{\partial\theta}{\partial X}\right)_{x=0} dy \tag{30}$$

3. Numerical approach and grid validation

A non – uniform structured grid of size 150 x 150 is used in this investigation and is revealed in Fig. 2. The number of grids in both X and Y directions are the same. To obtain accurate results, the calculations are performed by considering dissimilar grid sizes and adopted a grid size of 150 x 150 for all the simplifications of the current investigation. To authenticate the sturdiness of the current numerical procedure and the exactness of the outcomes, the results of current investigation are validated with existing works of Kahveci et al. [41] as shown in Table 2 and established better agreement.

The coupled governing Eqns. (18)–(20) along with boundary conditions (21) are mathematically calculated by employing Finite element procedure [42–45]. As the part of this method, firstly, the weak form of above equations is provided, later by employing Galerkin method these equations are discretized. By utilizing the equations weak form and by applying integration over the solution domain the residual equations are accomplished. Then, the subsequent set of residual algebraic equations is iteratively examined with the use of Newton method. The iterations are repeated until the residual error is less than 10^{-5}. Total computational procedure of these equations is implemented in Mathematica 10.0 package.

4. Results and discussion

This section provides the outcomes of thermal, hydrodynamic and heat capacity ratio of thermally radiative NEPCMs within a closed square chamber in terms of temperature lines, capacity ratio patterns and velocity lines in the form of contours are presented for several influenced parameters, such as, variable thermal conductivity parameter ($1 \le Nc \le 5$), variable viscosity parameter ($1 \le Nv \le 5$), radiation number ($0.1 \le R \le 0.5$), Rayleigh parameter $\left(10^2 \le Ra \le 10^3\right)$, volume fraction of NEPCMs ($1\% \le \phi \le 5\%$) and fusion temperature ($0.2 \le \theta_f \le 1.0$).

The significance of volume fraction of NEPCMs nano-particles (ϕ) on the contours of velocity lines (ψ), temperature lines (θ) and the patterns of heat capacity ratio (Cr) is exemplified from Figs. 3–5. As perceived, a single revolving cell is molded and the strength of this vortex intensifies

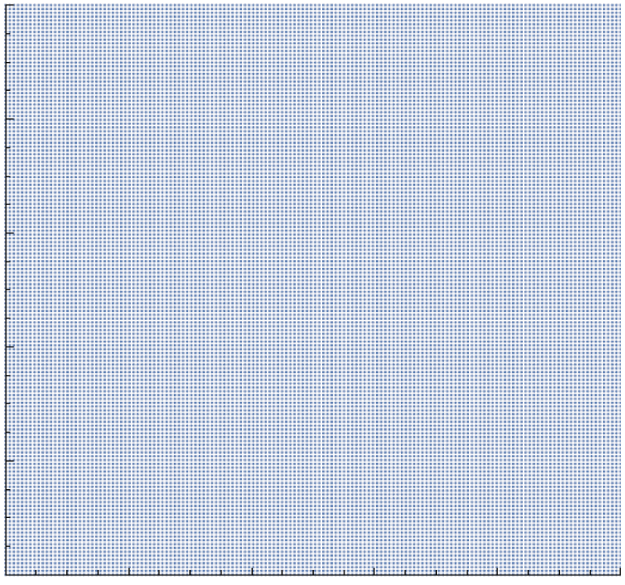

Fig. 2. The employed grid with size 150 x 150.

Table 2
Comparison of the results of Nusselt number with published work.

Parameter		Nusselt Number	
Ra	ϕ	Kahveci et al. [41]	Present study
10^6	0.0	9.20	9.22
10^6	0.05	9.76	9.73
10^6	0.1	10.3	10.31

in the center of the chamber with increasing values of (ϕ). The temperature of the liquid particles adjacent to the heated wall magnifies and travel up words, after that these particles travel parallel to the top wall until reaching the cooled wall, at the cold wall the temperature of these particles attenuates and moving down words. In this way convective flow generates which forms a convective cell with enlarging values of (ϕ) as depicted in Fig. 3. The temperature lines are highly affected by the convective flow and the curvedness of these lines magnifies with rising values of (ϕ) results amplification in temperature gradient values (Fig. 4). This is because; the suspension of NEPCMs in the base liquid magnifies the thermal conductivity and heat capacity of the nanoliquid as a consequence temperature gradient values magnifies with (ϕ). The patterns of heat capacity ratio (Cr) for diverse values of (ϕ) is depicted in Fig. 5. In this figure the white area is corresponding to the contours of (Cr) where the NEPCMs are at the fusion temperature and experiences change of phase from solid to liquid state inside their shells. Furthermore, the magnitude of phase change region attenuates within the chamber with rising (ϕ) values. Surely, phase change of core occurs if liquids temperature closed to the NEPCMs is greater than the NEPCMs fusion temperature.

Figs. 6–8 portray the effect of Rayleigh number (Ra) on the fields of velocity, isotherms and heat capacity ratio within the chamber. The liquid lines inside the chamber are nearly similar in all cases when (Ra) grows from 10^2 to 10^3 and formed a single revolving convective cell at the middle of the chamber. Additionally, the intensity of this vortex magnifies with escalating (Ra) values. The cause to increase vortex intensity is, raising the (Ra) values means forces of buoyancy are more dominating than the viscous forces as a result stronger convective cell is occurred. Rising values of (Ra) leads to form more number of temperature lines near the lowest corner of warm wall while the isotherms of lower temperature forms at the upper part of the cooled wall. Furthermore, the curvedness of these temperature lines magnifies with amplifying values of (Ra). The white colored area in the heat capacity ratio (Cr) fields in Fig. 8 is the area where the nanoparticles change its phase from solid to liquid. It also clear form this figure that the size of this area magnifies as (Ra) values amplifies. This means nanoparticles fusion temperature time marginally intensifies as the values of (Ra) grows from 10^2 to 10^3.

Radiation number (R) influence on the lines of velocity, temperature and heat capacity ratio is portrayed from Figs. 9–11. The lines of velocity are formed in a single convective recirculating cell and the flow rate magnifies with intensifying values of (R). Additionally, the vortex size amplifies as the (R) values rises from 0.1 to 0.5. The inclusion of (R) inside the flow field remarkably enhances the temperature of the liquid within the chamber. As a consequence more amount of heat transmitted from the warmth wall to cooled wall. Moreover, isotherms bowed ness considerably magnifies with higher (R) values. The size of the white colored area on the patterns of (Cr) deteriorates with increasing (R) values. This means the time of fusion temperature where the nanoparticles experiences change of phase from solid to fluid diminishes as the (R) values magnifies.

Figs. 12–14 portrays the patterns of streamlines, isotherms and the patterns of heat capacity ratio for altered values of dynamic viscosity parameter (Nv). Streamlines are formed in single vowel shaped convective cell and the intensity of this vortex diminishes as (Nv) values amplify. This type of nature in velocity lines is expected because

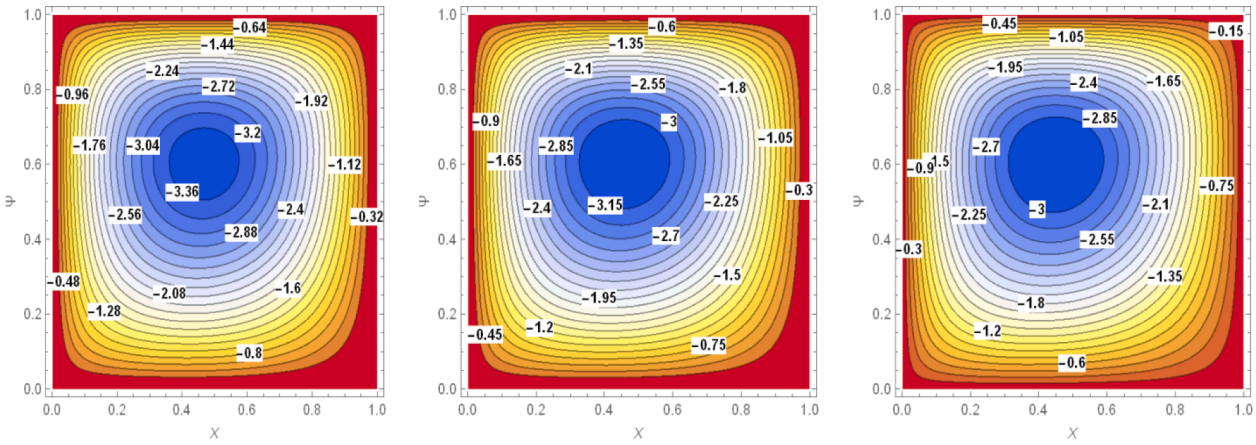

Fig. 3. Streamlines (ψ) with (ϕ) for Nc = 3.0, θ_f = 0.1, Ste = 0.3, Ra = 500, R = 0.5, Pr = 6.2, Nv = 3.0.

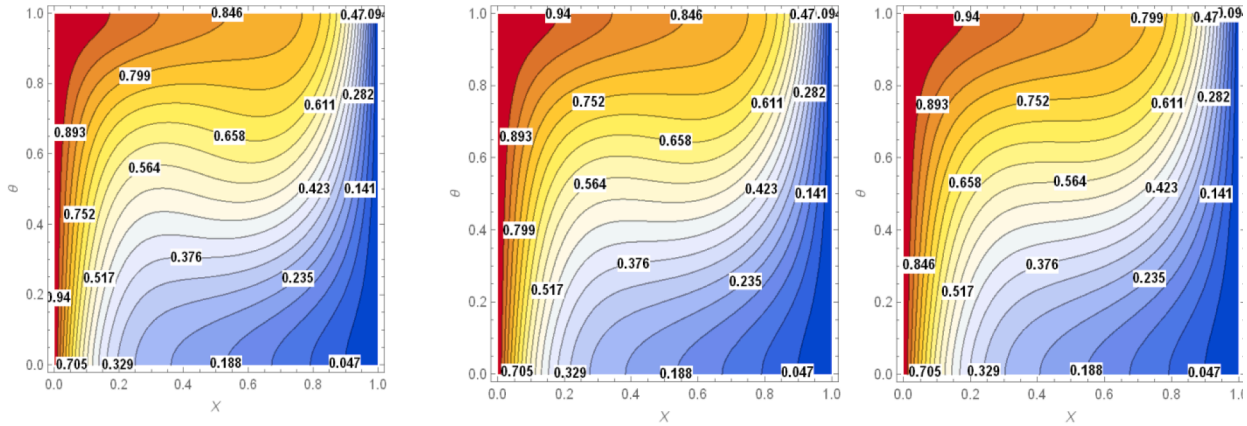

Fig. 4. Isotherms (θ) with (ϕ) for Nc = 3.0, θ_f = 0.1, Ste = 0.3, Ra = 500, R = 0.5, Pr = 6.2, Nv = 3.0.

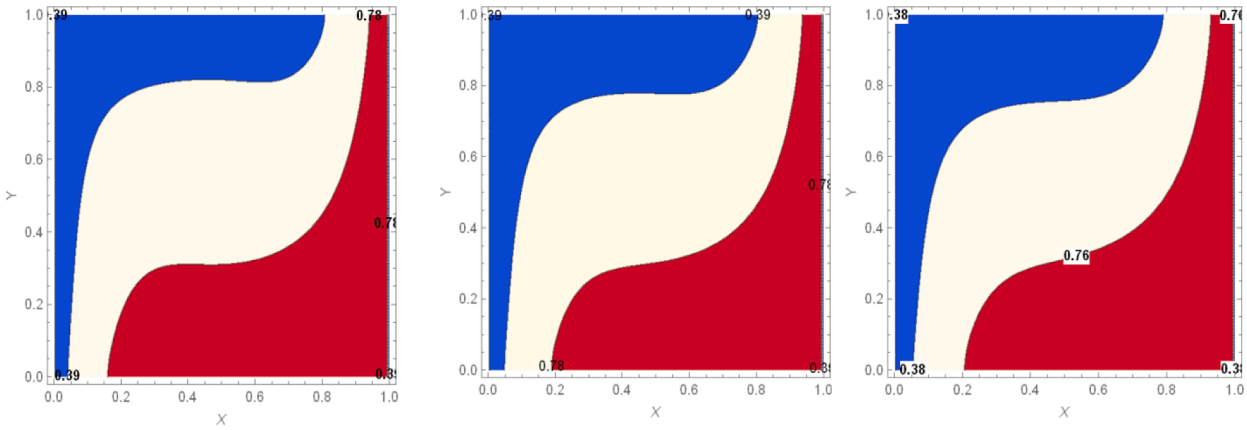

Fig. 5. Heat Capacity Ratio (Cr) with (ϕ) for Nc = 3.0, θ_f = 0.1, Ste = 0.3, Ra = 500, R = 0.5, Pr = 6.2, Nv = 3.0.

increasing (Nv) values means viscosity of the liquid intensifies causes denigration in the flow rate. The contours of isotherms are highly influenced by the (Nv). The isotherms line of θ = 0.047 is very near to the cooled wall with a marginal deviation at the lower part of the cold wall of the chamber, then, the isotherms line θ = 0.423 has larger deviation from the cold wall, in the center part of the chamber it is virtually parallel to bottom wall then reached to the hot wall. The value of heat capacity ratio (Cr) outside the fusion temperature area is 0.76. The area

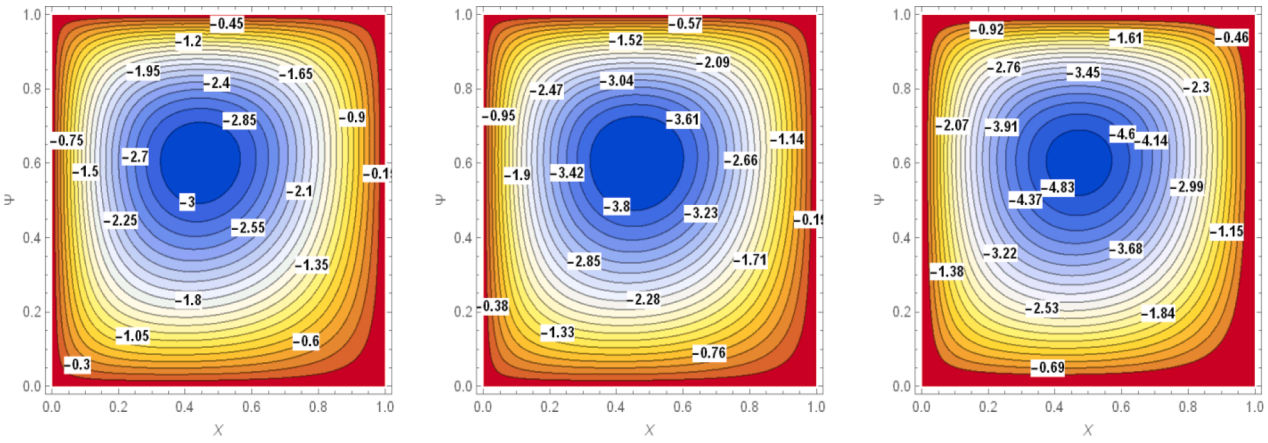

Fig. 6. Streamlines (ψ) with (Ra) for $Nc = 3.0, Pr = 6.2, \theta_f = 0.1, R = 0.5, Ste = 0.3, \phi = 0.01, Nv = 3.0$.

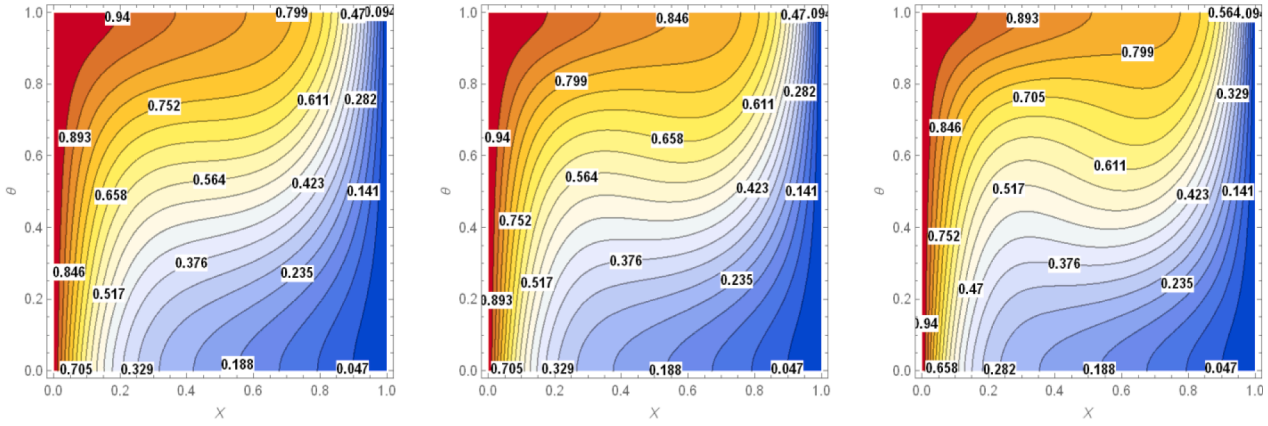

Fig. 7. Isotherms (θ) with (Ra) for $Nc = 3.0, Pr = 6.2, \theta_f = 0.1, R = 0.5, Ste = 0.3, \phi = 0.01, Nv = 3.0$.

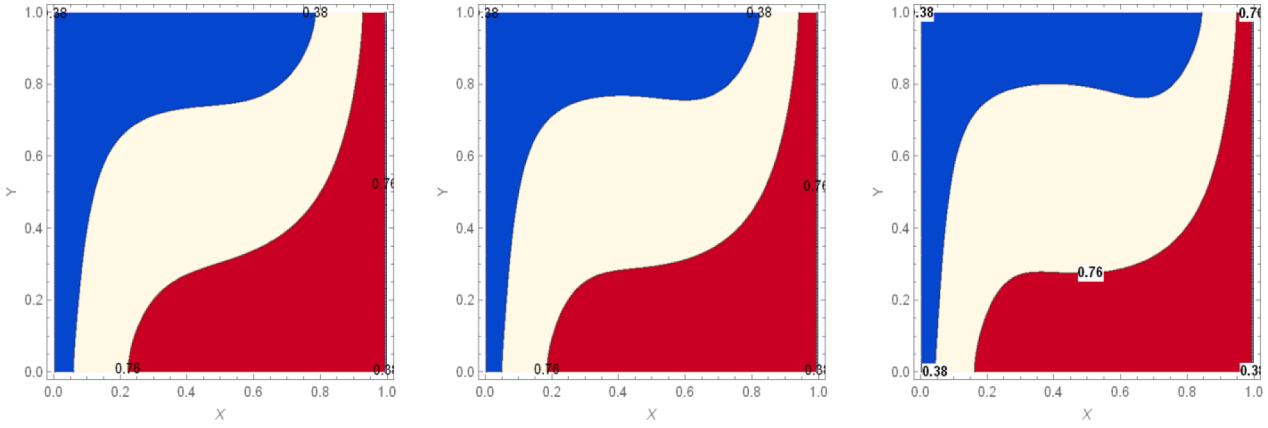

Fig. 8. Heat Capacity Ratio (Cr) with (Ra) for $Nc = 3.0, Pr = 6.2, \theta_f = 0.1, R = 0.5, Ste = 0.3, \phi = 0.01, Nv = 3.0$.

occupied by this fusion temperature region is larger at the center of the chamber, whereas, at the lower part and top of the chamber the area occupied by this fusion temperature is thinner and this white color area representing fusion temperature is like ribbon shape.

Figs. 15–17 interprets dissimilar values of dynamic thermal conductivity number (Nc) impact on the patterns of velocity lines, temperature lines and the contours of heat capacity ratio. A single revolving vowel shaped convective cell is formed and the intensity of this vortex

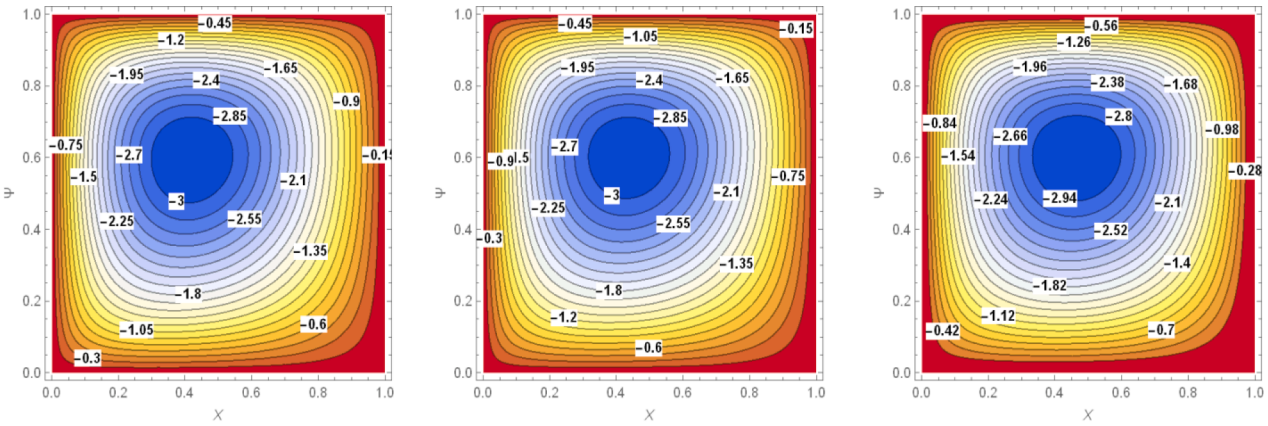

Fig. 9. Streamlines (ψ) with (R) for Nc = 3.0, θ_f = 0.1, Ste = 0.3, ϕ = 0.01, Ra = 500, Pr = 6.2, Nv = 3.0.

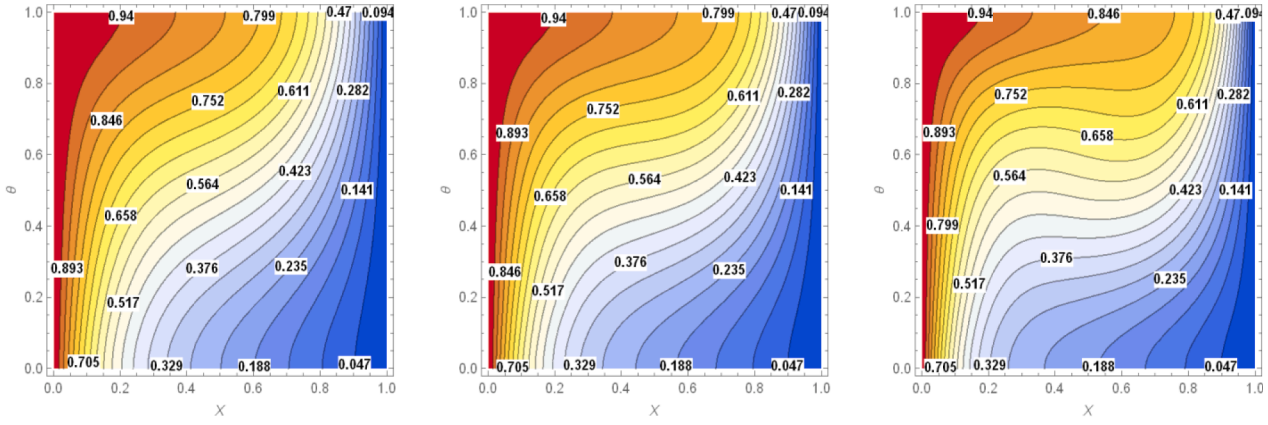

Fig. 10. Isotherms (θ) with (R) for Nc = 3.0, θ_f = 0.1, Ste = 0.3, ϕ = 0.01, Ra = 500, Pr = 6.2, Nv = 3.0.

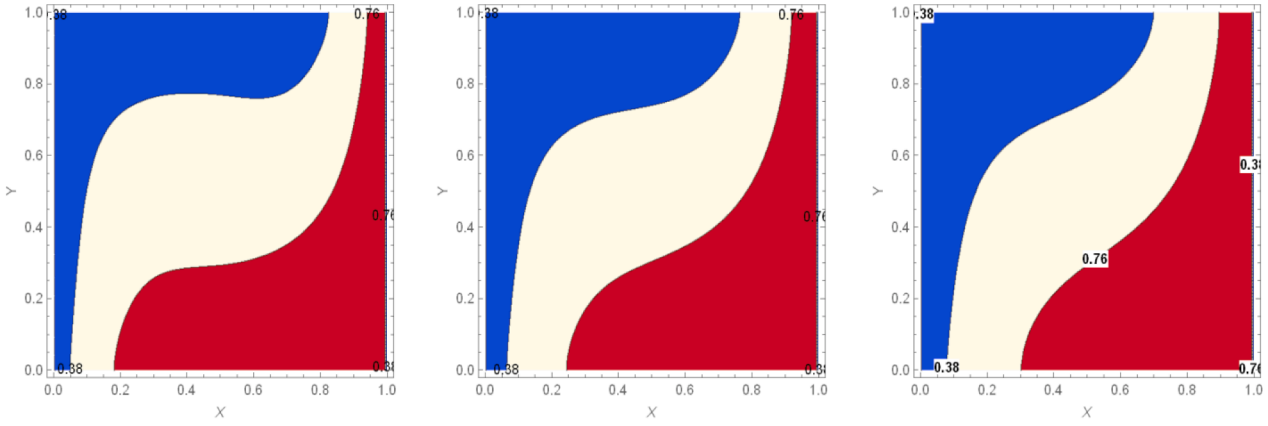

Fig. 11. Heat Capacity Ratio (Cr) with (R) for Nc = 3.0, θ_f = 0.1, Ste = 0.3, Nv = 3.0, ϕ = 0.01, Ra = 500, Pr = 6.2.

diminishes as (Nc) values amplify. The isotherms having higher temperature are closed formed at the lower area of warm wall, whereas, isotherms with lower temperature are thickly formed near the top of the cold wall. The heat capacity ratio (Cr) fields are formed like ribbon shape with color white. The area occupied by this fusion temperature region is larger at the center of the chamber and is weakens as the values of (Nc) magnifies, whereas, at the top and bottom of the cavity the area occupied by this fusion temperature is thinner and this white color area representing fusion temperature is like ribbon shape.

The sway of fusion temperature (θ_f) on the contours of velocity,

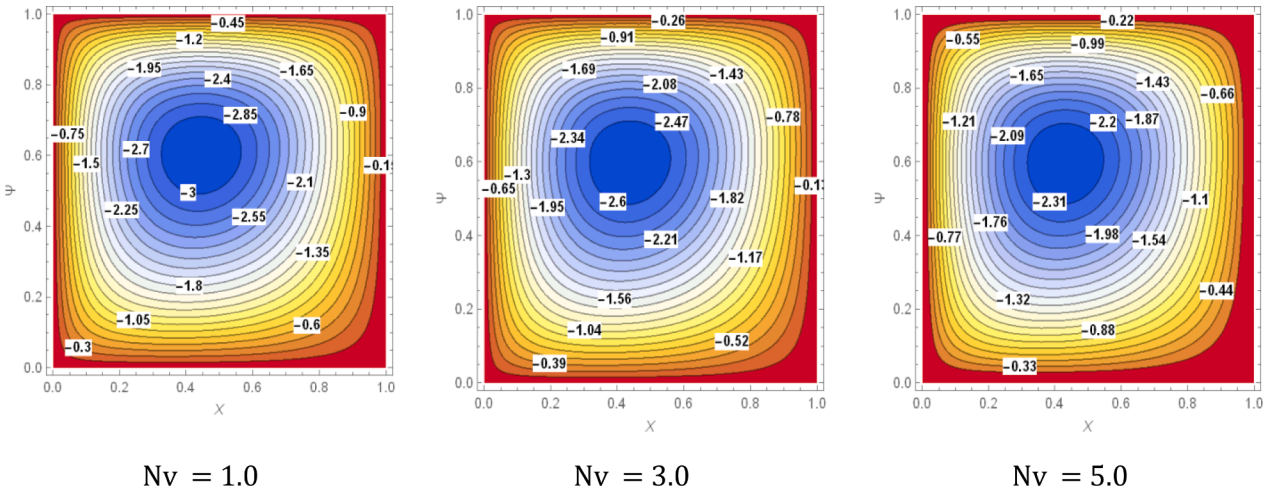

Fig. 12. Streamlines (ψ) with (Nv) for $Nc = 3.0, Pr = 6.2, \theta_f = 0.1, Ste = 0.3, R = 0.5, \phi = 0.01, Ra = 500$.

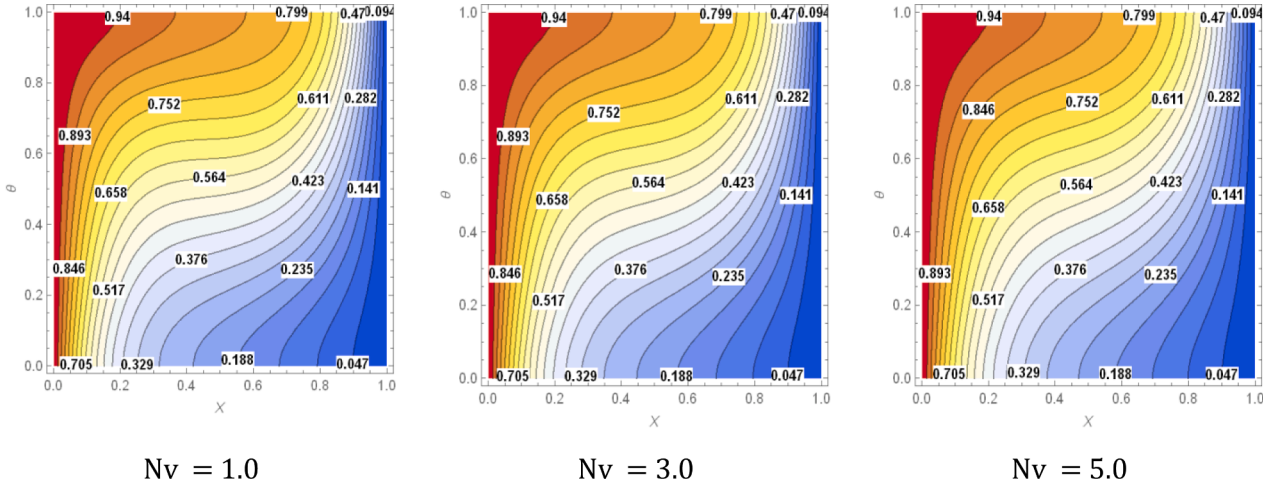

Fig. 13. Isotherms (θ) with (Nv) for $Nc = 3.0, Pr = 6.2, \theta_f = 0.1, Ste = 0.3, R = 0.5, \phi = 0.01, Ra = 500$.

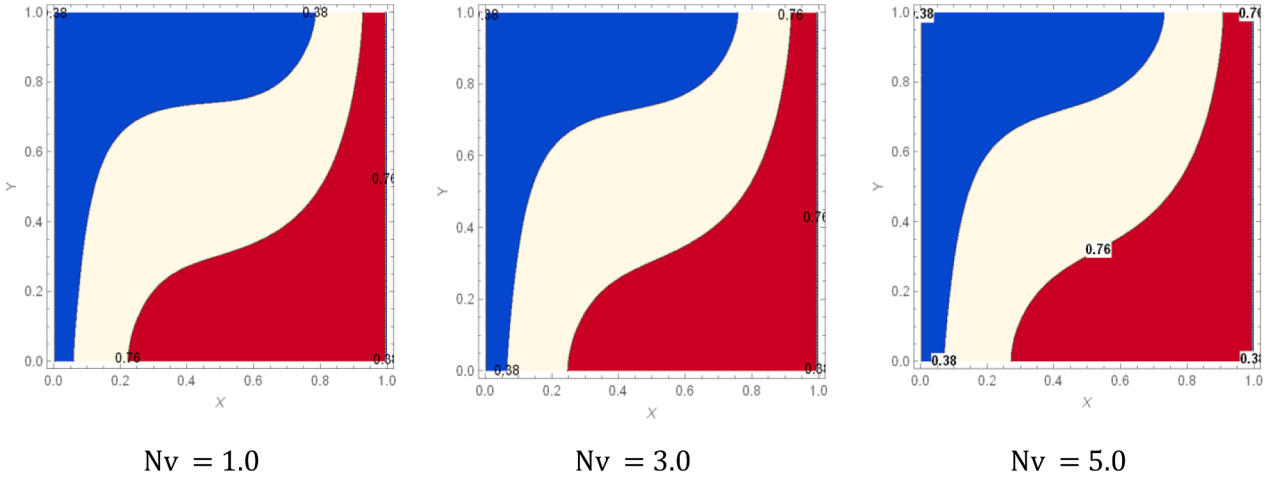

Fig. 14. Heat Capacity Ratio (Cr) with (Nv) for $Nc = 3.0, \theta_f = 0.1, Ste = 0.3, \phi = 0.01, R = 0.5, Pr = 6.2, Ra = 500$.

temperature lines and heat capacity ratio of nanoliquid is portrayed from Figs. 18–20. As the values of (θ_f) intensifies from 0.1 to 0.9, a single revolving convective vortex is molded and the intensity of this vortex denigrates. The reason for this behavior of streamlines is liquid temperature is almost constant during the change of phase of NEPCM as a result there is a deterioration in the buoyancy forces of the liquid causes to denigration in the intensity of the streamlines. With magnification in the (θ_f) values the thermal conductivity of the nanoliquid

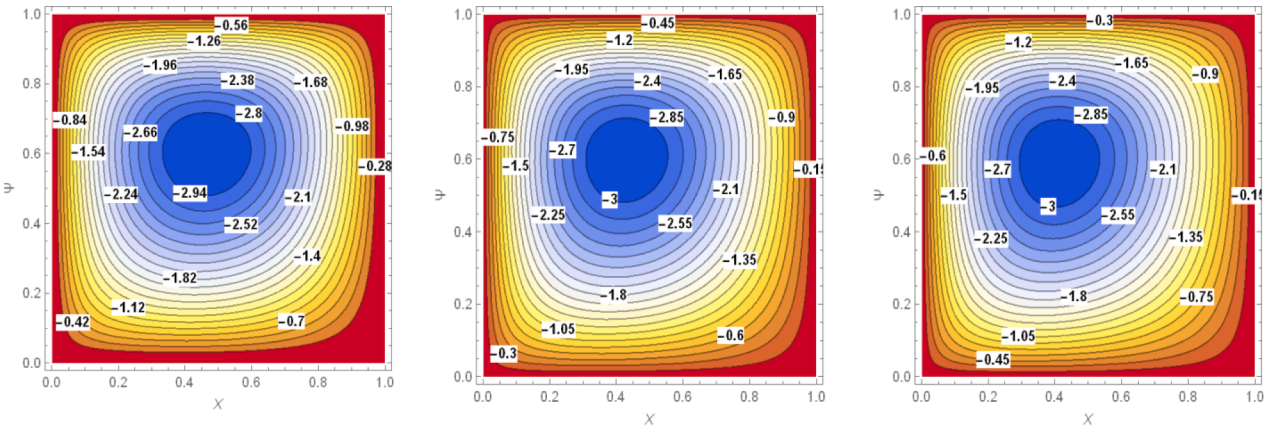

Fig. 15. Streamlines (ψ) with (Nc) for Nv = 3.0, R = 0.5, θ_f = 0.1, Ste = 0.3, Pr = 6.2, ϕ = 0.01, Ra = 500.

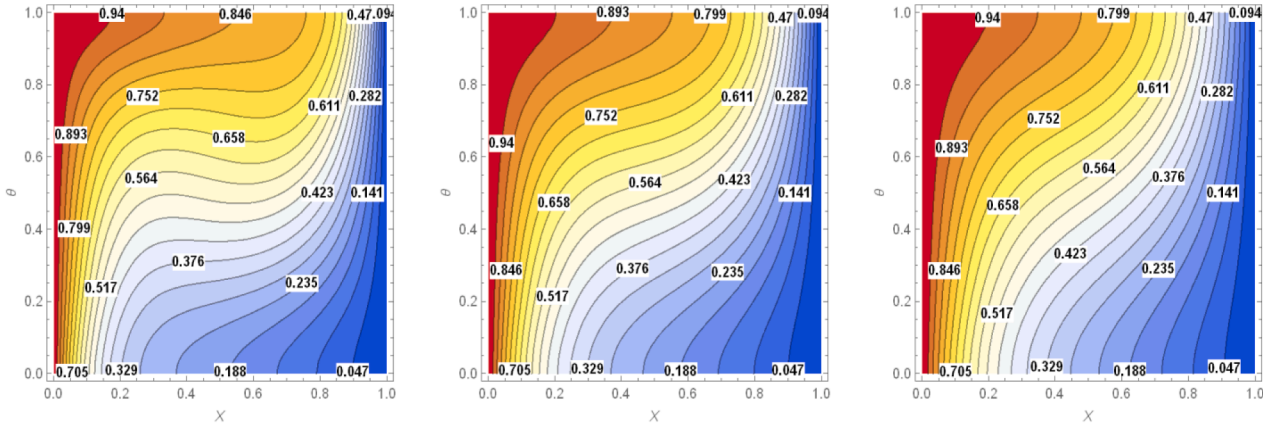

Fig. 16. Isotherms (θ) with (Nc) for Nv = 3.0, R = 0.5, θ_f = 0.1, Ste = 0.3, Pr = 6.2, ϕ = 0.01, Ra = 500.

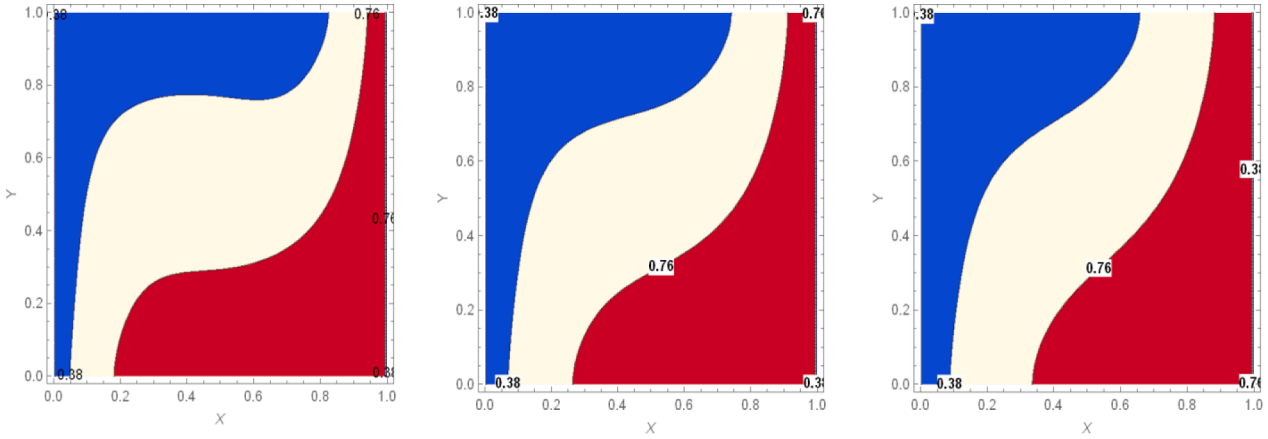

Fig. 17. Heat Capacity Ratio (Cr) with (Nc) for Nv = 3.0, R = 0.5, θ_f = 0.1, Ste = 0.3, Pr = 6.2, ϕ = 0.01, Ra = 500.

amplifies results higher conduction mechanism of the liquid. As the consequence of this higher heat conduction process more amount of liquid moves from warm wall to cooled wall results horizontal shape of isotherms in the middle of the cavity. The white color area in the heat capacity ratio figures represents the time taken by the nanoparticles to transform its phase from solid to fluid. Whenever the fusion temperature is minimum there exists higher temperature gradient between the solid and hot wall as a consequence rates of heat transport is more compared

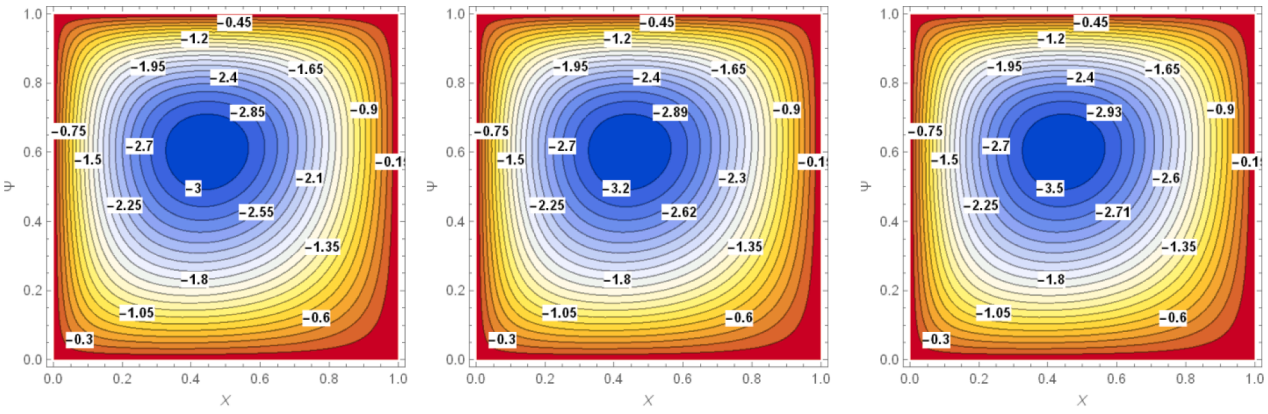

$\theta_f = 0.1$ $\theta_f = 0.4$ $\theta_f = 0.7$

Fig. 18. Streamlines (ψ) with (θ_f) for $Nv = 3.0, R = 0.5, Ste = 0.3, Nc = 3.0, Pr = 6.2, \phi = 0.01, Ra = 500$.

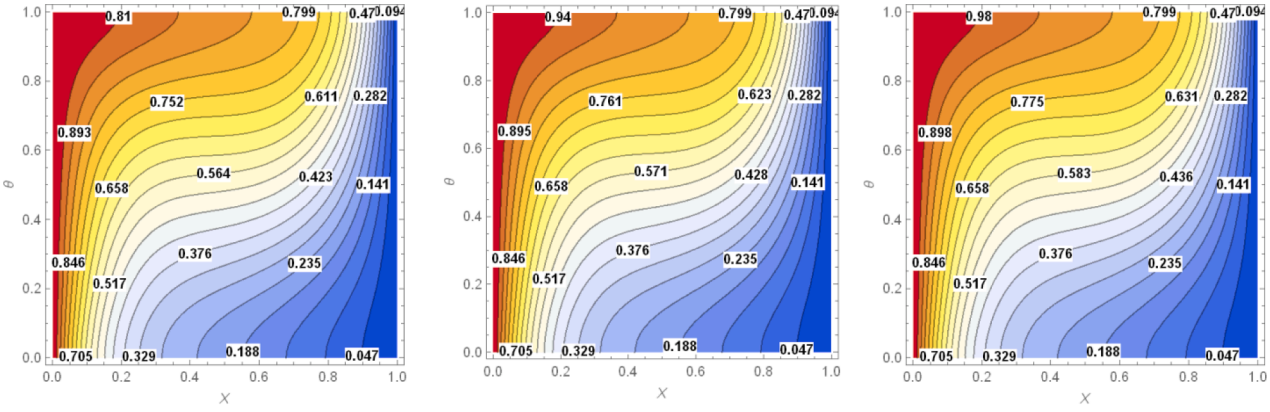

$\theta_f = 0.1$ $\theta_f = 0.4$ $\theta_f = 0.7$

Fig. 19. Isotherms (θ) with (θ_f) for $Nv = 3.0, R = 0.5, Ste = 0.3, Nc = 3.0, Pr = 6.2, \phi = 0.01, Ra = 500$.

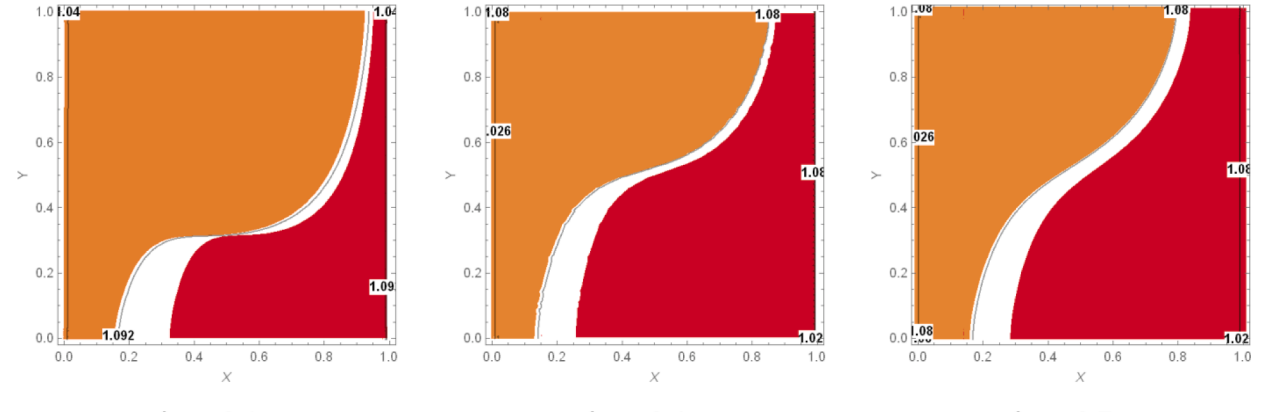

$\theta_f = 0.1$ $\theta_f = 0.4$ $\theta_f = 0.7$

Fig. 20. Heat Capacity Ratio (Cr) with (θ_f) for $Nv = 3.0, R = 0.5, Ste = 0.3, Nc = 3.0, Pr = 6.2, \phi = 0.01, Ra = 500$.

to the higher fusion temperature.

Figs. 21 and 22 shows the Nusselt number profiles at both cold and hot walls for different values of (ϕ). As seen, by augmenting the (ϕ) values the non – dimensional rates of heat transport at both cold and hot walls magnifies inside the cavity. It is true because increasing the (ϕ) values boost the thermal conductivity of the NEPCM leads to augmentation in heat transport rates. Values of Nusselt number at both cold and hot walls denigrates with increasing values of (Ra) as illustrated in Figs. 23 and 24. This is because viscous effects are almost negligible when the (Ra) values augment which causes the deterioration in the heat transport rates. As seen from Figs. 25 & 26, the non – dimensional heat transport rates at both walls magnifies with amplifying (R) values. It is perceived from Figs. 27 and 28 that Stefan number (Ste) magnifies the heat transport rate of NEPCM inside the cavity. As deliberated earlier, at

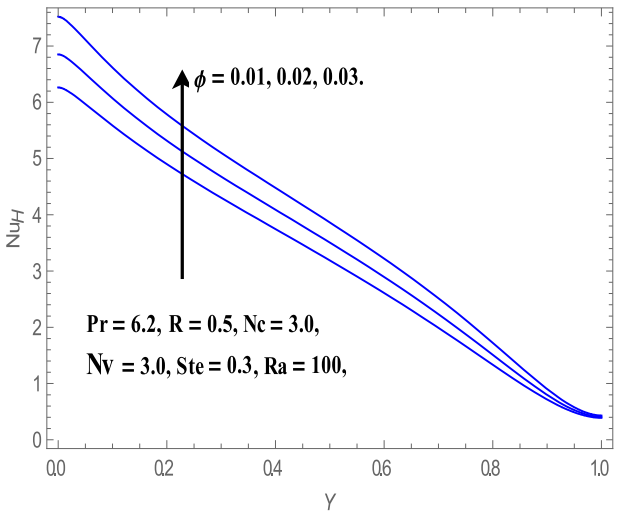

Fig. 21. Significance of (ϕ) on (Nu) at hot wall.

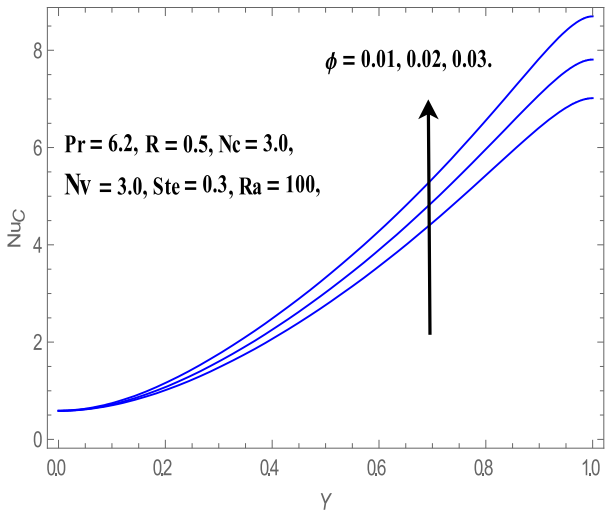

Fig. 22. Significance of (ϕ) on (Nu) at cold wall.

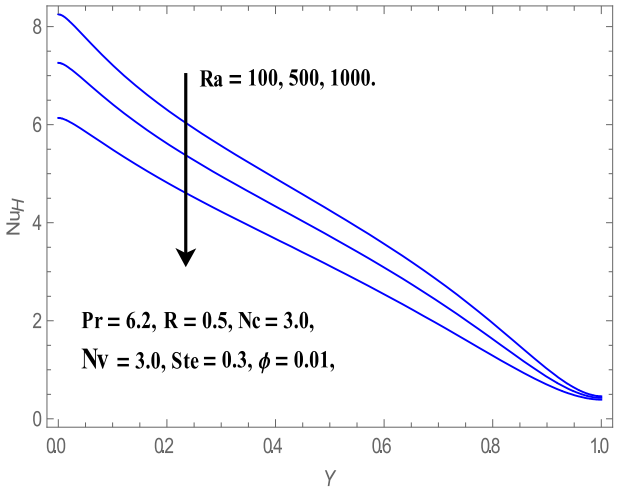

Fig. 23. Significance of (Ra) on (Nu) at hot wall.

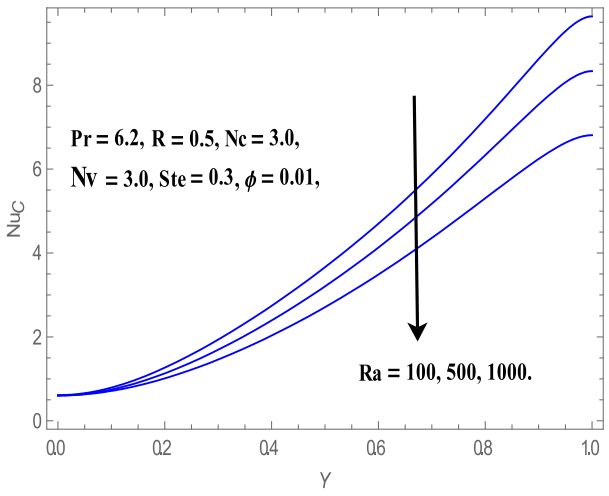

Fig. 24. Significance of (Ra) on (Nu) at cold wall.

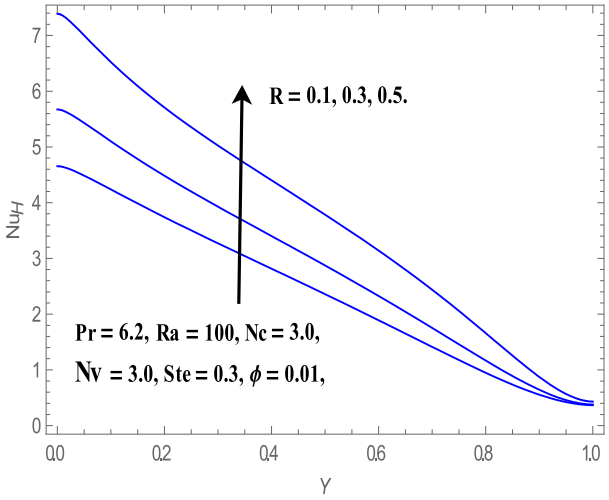

Fig. 25. Significance of (R) on (Nu) at hot wall.

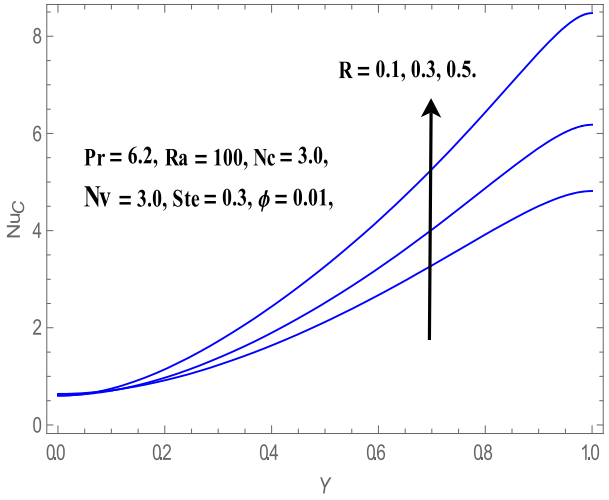

Fig. 26. Significance of (R) on (Nu) at cold wall.

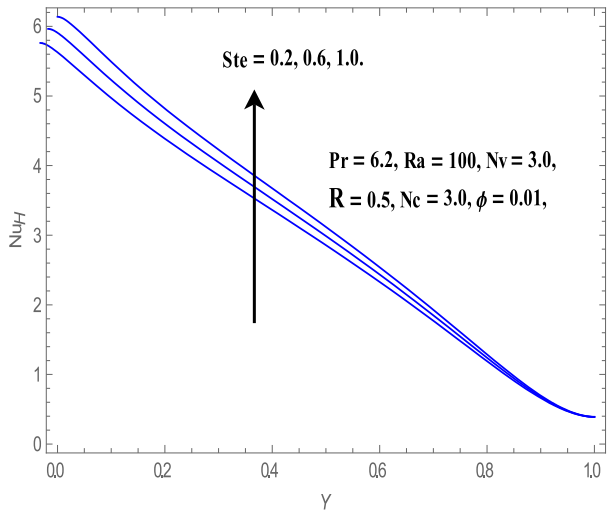

Fig. 27. Significance of (Ste) on (Nu) at hot wall.

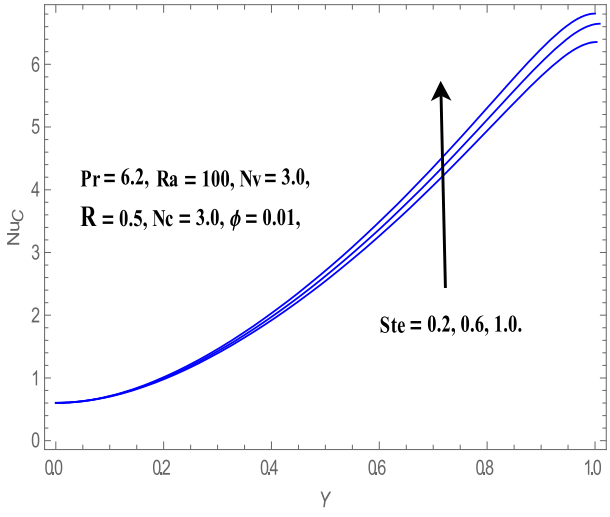

Fig. 28. Significance of (Ste) on (Nu) at cold wall.

the lower values of Stefan number highest rates of heat transport achieved.

5. Conclusion

Thermally radiative NEPCMs heat transport and flow features over a closed chamber is numerically scrutinized in this analysis. The capsules are prepared with a shell and a phase change material as core. Shell prevents the phase change materials from the hot fluid and leakage. To examine the equations representing liquid flow and energy, a versatile Finite element analysis was implemented. The imperative deductions of the present analysis are précised below.

(i) As the values of (θ_f) magnifies, the area occupied by the white region in the contours of heat capacity ratio denigrates. This means NEPCMs has taken less time to transform its phase from solid to fluid.
(ii) Non – dimensional rates of heat transport magnifies with growing (Ste) values.
(iii) As the volume fraction NEPCMs values amplify from 1 % to 5 % the heat transport rates of the nanoliquid magnifies 42% compared to the host fluid.
(iv) Intensity of the patterns of velocity attenuates within the chamber with increasing values of (Nv).
(v) The area occupied by this fusion temperature region is larger at the center of the cavity and is diminishes as the values of (Nc) amplifies.

CRediT authorship contribution statement

P. Sudarsana Reddy: Formal analysis, Data curation, Conceptualization. **P. Sreedevi:** Software, Resources, Methodology. **Mohammad Ghalambaz:** Visualization, Validation, Supervision.

Declaration of competing interest

The authors declare that they have no known competing financial interests or personal relationships that could have appeared to influence the work reported in this paper.

Data availability

Data will be made available on request.

References

[1] A.J. Chamkha, T. Armaghani, M.A. Mansour, A.M. Rashad, H. Kargarsharifabad, MHD convection of an Al2O3-Cu/Water hybrid nanofluid in an inclined porous cavity with internal heat generation/absorption, Iran. J. Chem. Chem. Eng. 41 (2021) (3), 936–956.
[2] A. Chamkha, Z. Abdelrahman, M. Mansour, T. Armaghani, A. Rashad, Effects of magnetic field inclination and internal heat sources on nanofluid heat transfer and entropy generation in a double lid driven L-shaped cavity, Therm. Sci. 25 (2) (2021) 1033–1046.
[3] M. Ghalambaz, S.M. Hashem Zadeh, A. Veismoradi, M.A. Sheremet, I. Pop, Free convection heat transfer and entropy generation in an odd-shaped cavity filled with a Cu-Al2O3 hybrid nanofluid, Symmetry 13 (1) (2021) 122.
[4] A.I. Alsabery, I. Hashim, A. Hajjar, M. Ghalambaz, S. Nadeem, M. Saffari Pour, Entropy generation and natural convection flow of hybrid nanofluids in a partially divided wavy cavity including solid blocks, Energies 13 (11) (2020) 2942.
[5] P. Sreedevi, P. Sudarsana Reddy, M.A. Sheremet, Impact of homogeneous–heterogeneous reactions on heat and mass transfer flow of Au–Eg and Ag–Eg Maxwell nanofluid past a horizontal stretched cylinder, J. Therm. Anal. Calorim. 141 (1) (2020) 533–546.
[6] P. Sreedevi, P. Sudarsana Reddy, Combined influence of brownian motion and thermophoresis on Maxwell three-dimensional nanofluid flow over stretching sheet with chemical reaction and thermal radiation, J. Porous Media 23 (4) (2020) 327–340.
[7] M.A. Sheremet, H.F. Öztop, Impact of porous complicated fin and sinusoidal-heated wall on thermogravitational convection of different nanofluids in a square domain, Int. J. Therm. Sci. 168 (2021) 107053.
[8] M.A. Sheremet, M.M. Rashidi, Thermal convection of nano-liquid in an electronic cabinet with finned heat sink and heat generating element, Alex. Eng. J. 60 (3) (2021) 2769–2778.
[9] P. Sudarsana Reddy, P. Sreedevi, S. Venkateswarlu, Impact of modified Fourier's heat flux on the heat transfer of MgO/Fe3O4–Eg-based hybrid nanofluid flow inside a square chamber, Waves Random Complex Media 1–23 (2022), https://doi.org/10.1080/17455030.2022.2058112.
[10] P. Sudarsana Reddy, P. Sreedevi, A.J. Chamkha, Hybrid nanofluid heat and mass transfer characteristics over a stretching/shrinking sheet with slip effects, J. Nanofluids 12 (1) (2023) 251–260.
[11] F. Selimefendigil, H.F. Öztop, Natural convection and melting of NEPCM in a corrugated cavity under the effect of magnetic field, J. Therm. Anal. Calorim. 140 (3) (2019) 1427–1442.
[12] M. Ghalambaz, S.A.M. Mehryan, A. Hajjar, A. Veismoradi, Unsteady natural convection flow of a suspension comprising Nano-Encapsulated Phase Change Materials (NEPCMs) in a porous medium, Adv. Powder Technol. 31 (3) (2020) 954–966.
[13] P.M. Kumar, K. Mylsamy, A comprehensive study on thermal storage characteristics of nano-CeO2 embedded phase change material and its influence on the performance of evacuated tube solar water heater, Renew. Energy 162 (2020) 662–676.
[14] A. Sathishkumar, M. Cheralathan, Influence of thermal transport properties of NEPCM for cool thermal energy storage system, J. Therm. Anal. Calorim. 147 (1) (2020) 367–378.
[15] S.R. Afshar, S.R. Mishra, A.S. Dogonchi, N. Karimi, A.J. Chamkha, H. Abulkhair, Dissection of entropy production for the free convection of NEPCMs-filled porous wavy enclosure subject to volumetric heat source/sink, J. Taiwan Inst. Chem. Eng. 128 (2021) 98–113.
[16] M.K. Nayak, A.S. Dogonchi, Y. Elmasry, N. Karimi, A.J. Chamkha, H. Alhumade, Free convection and second law scrutiny of NEPCM suspension inside a wavy-

baffle-equipped cylinder under altered Fourier theory, J. Taiwan Inst. Chem. Eng. 128 (2021) 288–300.
[17] H. Peng, J. Wang, X. Zhang, J. Ma, T. Shen, S. Li, B. Dong, A review on synthesis, characterization and application of nanoencapsulated phase change materials for thermal energy storage systems, Appl. Therm. Eng. 185 (2021) 116326.
[18] S.M. Seyyedi, M. Hashemi-Tilehnoee, M. Sharifpur, Effect of inclined magnetic field on the entropy generation in an annulus filled with NEPCM Suspension, Math. Probl. Eng. 2021 (2021) 1–14.
[19] W. Lan, B. Shang, R. Wu, X. Yu, R. Hu, X. Luo, Thermally-enhanced nanoencapsulated phase change materials for latent functionally thermal fluid, Int. J. Therm. Sci. 159 (2021) 106619.
[20] A. Alhashash, H. Saleh, Impact of surface undulation on flow and heat transfer characteristics in an enclosure filled with nanoencapsulated phase change materials (NEPCMs), Math. Probl. Eng. 2021 (2021) 1–13.
[21] A.M. Aly, S.E. Ahmed, ISPH simulations of convective flow within a porous circular cylinder over a rectangular cavity containing nano-encapsulated phase change materials (NEPCMs), Phys. Scr. 96 (10) (2021) 105211.
[22] A.S. Dogonchi, S.R. Mishra, N. Karimi, A.J. Chamkha, H. Alhumade, Interaction of fusion temperature on the magnetic free convection of nano-encapsulated phase change materials within two rectangular fins-equipped porous enclosure, J. Taiwan Inst. Chem. Eng. 124 (2021) 327–340.
[23] W.Q. Li, S.J. Guo, L. Tan, L.L. Liu, W. Ao, Heat transfer enhancement of nano-encapsulated phase change material (NEPCM) using metal foam for thermal energy storage, Int. J. Heat Mass Transf. 166 (2021) 120737.
[24] M. Alizadeh, A. Nabizadeh, A. Fazlollahtabar, D.D. Ganji, An optimization study of solidification procedure in a wavy- wall storage unit considering the impacts of NEPCM and curved fin, Int. Commun. Heat Mass Transfer 124 (2021) 105249.
[25] A.M. Zidan, M.K. Nayak, N. Karimi, A. Sattar Dogonchi, A.J. Chamkha, M.B. Ben Hamida, A.M. Galal, Thermal management and natural convection flow of nano encapsulated phase change material (NEPCM)-water suspension in a reverse T-shaped porous cavity enshrining two hot corrugated baffles: A boost to renewable energy storage, J. Build. Eng. 53 (2022) 104550.
[26] A.M. Aly, A.-A. Hyder, N. Alsedias, Time-Conformable fractal systems of natural convection of tall fin inside two circular cylinders suspended by NEPCM, Alex. Eng. J. 61 (12) (2022) 12311–12328.
[27] S. Doshi, G. Kashyap, N. Tiwari, Thermo-hydraulic and entropy generation investigation of nano-encapsulated phase change material (NEPCM) slurry in hybrid wavy microchannel, Int. J. Numer. Meth. Heat Fluid Flow 32 (10) (2022) 3161–3190.
[28] S. Mandal, S. Ishak, J.K. Singh, D.-E. Lee, T. Park, Synthesis and application of paraffin/silica phase change nanocapsules: Experimental and numerical approach, J. Storage Mater. 51 (2022) 104407.
[29] S. Hussain, Z. Raizah, A.M. Aly, Thermal radiation impact on bioconvection flow of nano-enhanced phase change materials and oxytactic microorganisms inside a vertical wavy porous cavity, Int. Commun. Heat Mass Transfer 139 (2022) 106454.
[30] E.J. D'Oliveira, S.C.C. Pereira, D. Groulx, U. Azimov, Thermophysical properties of Nano-enhanced phase change materials for domestic heating applications, J. Storage Mater. 46 (2022) 103794.
[31] M. Ghalambaz, H. Jin, A. Bagheri, O. Younis, D. Wen, Convective flow and heat transfer of nano-encapsulated phase change material (NEPCM) dispersions along a vertical surface, Facta Universitatis, Series: Mech. Eng. 20 (3) (2022) 519.
[32] M. Ghalambaz, S.A.M. Mehryan, M. Vaezi, I. Zahmatkesh, A. Hajjar, O. Younis, M. Ghalambaz, Unsteady natural convection of nano-encapsulated phase change materials (NEPCMs) inside a random porous medium considering local thermal non-equilibrium condition, Waves Random Complex Media 1–22 (2022), https://doi.org/10.1080/17455030.2022.2088893.
[33] M. Khodadadi, M. Sheikholeslami, Heat transfer efficiency and electrical performance evaluation of photovoltaic unit under influence of NEPCM, Int. J. Heat Mass Transf. 183 (2022) 122232.
[34] M.S. Sadeghi, A.J. Chamkha, R. Ali, M.B. Ben Hamida, M. Ghodrat, A.M. Galal, Hydrothermal behavior of micro-polar Nano-Encapsulated phase change materials (NEPCMs) in an inclined L-shaped cavity, Case Stud. Therm. Eng. 35 (2022) 102039.
[35] N. Radhakrishnan, C.B. Sobhan, Thermophysical characterization and melting heat transfer analysis of an organic phase change material dispersed with GNP- Ag hybrid nanoparticles, Heat Mass Transf. 58 (10) (2022) 1811–1828.
[36] Y. Zhuang, H. Li, W. Xu, S.-M. Huang, Experimental study on the melting performance of magnetic NEPCMs embedded in metal foam subjected to a non-uniform magnetic field, Sol. Energy Mater. Sol. Cells 250 (2023) 112077.
[37] Q. Wang, L. Yang, J. Song, Preparation, thermal conductivity, and applications of nano–enhanced phase change materials (NEPCMs) in solar heat collection: A review, J. Storage Mater. 63 (2023) 107047.
[38] J. Zhang, Z. Cheng, Y. Zhou, B. Lu, Y. Zhang, Numerical study using lattice Boltzmann method on melting and solidification of NEPCM placed inside a rectangular cavity with a new double-fin arrangement, Appl. Therm. Eng. 219 (2023) 119619.
[39] M. Ghalambaz, M. Aljaghtham, A.J. Chamkha, A. Abdullah, U. Alqsair, M. Ghalambaz, Dynamic melting in an open enclosure supported by a partial layer of metal foam: A fast thermal charging approach, Int. J. Heat Mass Transf. 203 (2023) 123760.
[40] J. Shafi, M. Sheremet, M. Fteiti, A.M. Saeed, M. Ghalambaz, Computational study of phase change heat transfer and latent heat energy storage for thermal management of electronic components using neural networks, Mathematics 11 (2) (2023) 356.
[41] K. Kahveci, Buoyancy driven heat transfer of nanofluids in a tilted enclosure, J. 947, Heat Transf. 132 (2010) 062501.
[42] P. Sudarsana Reddy, A.J. Chamkha, Soret and Dufour Effects on unsteady MHD heat and mass transfer over a stretching sheet with thermophoresis and non-uniform heat generation/absorption, J. Appl. Fluid Mech. 9 (2016) 2443–2455.
[43] P. Sreedevi, P. Sudarsana Reddy, Ali J. Chamkha, Heat and Mass transfer analysis of nanofluid over linear and non- linear stretching surface with thermal radiation and chemical reaction, Powder Technol. 315 (2017) 194–204.
[44] P. Sudarsana Reddy, A.J. Chamkha, A.F. Al-mudhaf, MHD heat and mass transfer flow of a nanofluid over an inclined vertical porous plate with radiation and heat generation/absorption, Adv. Powder Technol. 28 (2017) 1008–1017.
[45] P. Sudarsana Reddy, K. Jyothi, M. Suryanarayana Reddy, Flow and heat transfer analysis of carbon nanotubes based maxwell nanofluid flow driven by rotating stretchable disks with thermal radiation, J. Braz. Soc. Mech. Sci. Eng. 40 (2018), 576, Doi: 10.1007/s40430-018-1494-9.